Multi-conjugate Adaptive Optics at Big Bear Solar Observatory

Dirk Schmidt[1], Nicolas Gorceix[2], Jose Marino[1],
Xianyu Zhang[4], Thomas Rimmele[1], Thomas Berkefeld[3], Phil Goode[2]

[1)] National Solar Observatory, 3665 Discovery Drive, Boulder, CO 80303, USA
[2)] Big Bear Solar Observatory, 40386 North Shore Lane, Big Bear City, CA 92315, USA
[3)] Kiepenheuer-Institut für Sonnenphysik, Schöneckstr. 6, 79104 Freiburg, Germany
[4)] Large Binocular Telescope Observatory, 933 N. Cherry Ave, Tucson, AZ 85721, USA

ABSTRACT

A multi-conjugate adaptive optics (MCAO) system for solar observations has been set up at the 1.6-meter clear aperture New Solar Telescope (NST) in Big Bear Lake, California. Being a pathfinder to address fundamental design questions in solar MCAO experimentally, the system is purposely flexible. We deploy three deformable mirrors (DMs). One of which is conjugate to the telescope pupil, and the other two to distinct higher altitudes. The pupil DM can be either placed into a pupil image up- or downstream of the high-altitude DMs. The high-altitude DMs can be separately and quickly conjugated to various altitudes between 2 and 8 km. Three Shack-Hartmann wavefront sensor units are available, one for low-order, multi-directional sensing and two high-order on-axis sensing of which one is used at a time. The flexibility of the setup allows us to experimentally study the various sequencings of DMs and WFSs, which are hard to simulate conclusively. We report on the preliminary results and summarize the design and the configuration options of the MCAO system at Big Bear Solar Observatory (BBSO).

Keywords: solar adaptive optics, multi-conjugate adaptive optics, MCAO, New Solar Telescope, KAOS Evo 2

1. INTRODUCTION AND MOTIVATION

MCAO is a technology pursued by ground-based solar observatories with the aim of implementing a tool to enlarge the field of view that is corrected for atmospheric turbulence as compared to classical adaptive optics (CAO). CAO systems deliver their best correction across a field of some seconds of arc (depending on the seeing conditions). Solar active regions, however, span tens of arcseconds. For fundamental understanding of the development and evolution of solar activity, observations with both high spatial and temporal resolution are essential. A wider corrected field of view would allow one to capture the solar surface in great detail at the very same instant. This is important because the target structures evolve quickly and the acquisition times of the instruments are typically too long to scan across active regions with a CAO system.

Solar MCAO has been investigated since the early 2000's,[1–3] and 2nd generation experimental MCAO systems have been set up in 2013 at the currently highest resolving power telescopes, the 1.6-meter New Solar Telescope (NST) of BBSO, and the 1.5-meter GREGOR of the Kiepenheuer-Institute.[4,5] MCAO is considered an integral part of the proposed European Solar Telescope (EST), and NSO's Daniel K. Inouye Solar Telescope (DKIST, formerly ATST), which is under construction on Maui and should be upgraded with MCAO once demonstrably successful designs for solar science have been implemented.

Send correspondence via e-mail to Dirk Schmidt (dschmidt@nso.edu)

2. MCAO AT BBSO

The MCAO project at BBSO is a collaboration of the U.S. National Solar Observatory (NSO), BBSO (operated by the New Jersey Institute of Technology), and the Kiepenheuer-Institut für Sonnenphysik (KIS). The scope of the current project is to demonstrate the value of MCAO for solar science using the 1.6-meter NST at BBSO, and to establish an experimental platform as the pathfinder system for the future MCAO system of DKIST. The NST is a 1.6-meter solar telescope with a clear aperture, off-axis design like the 4-meter DKIST. The absence of spiders in the aperture is a great advantage for adaptive optics, as spiders easily degrade the solar image in the small subapertures of the Shack-Hartmann wavefront sensors. Hence, the NST allows us to concentrate on MCAO difficulties with no need to worry about additional complications caused by spiders.

2.1 The NST MCAO system

MCAO is a new technology for daytime astronomy, and as such, merits careful study, especially since the key technical issues (wavefront sensing) and the targeted wavelength regimes are different than those for nighttime astronomy. The NST MCAO system, shown in fig. 1, is meant to be the pathfinder for DKIST MCAO. Thus

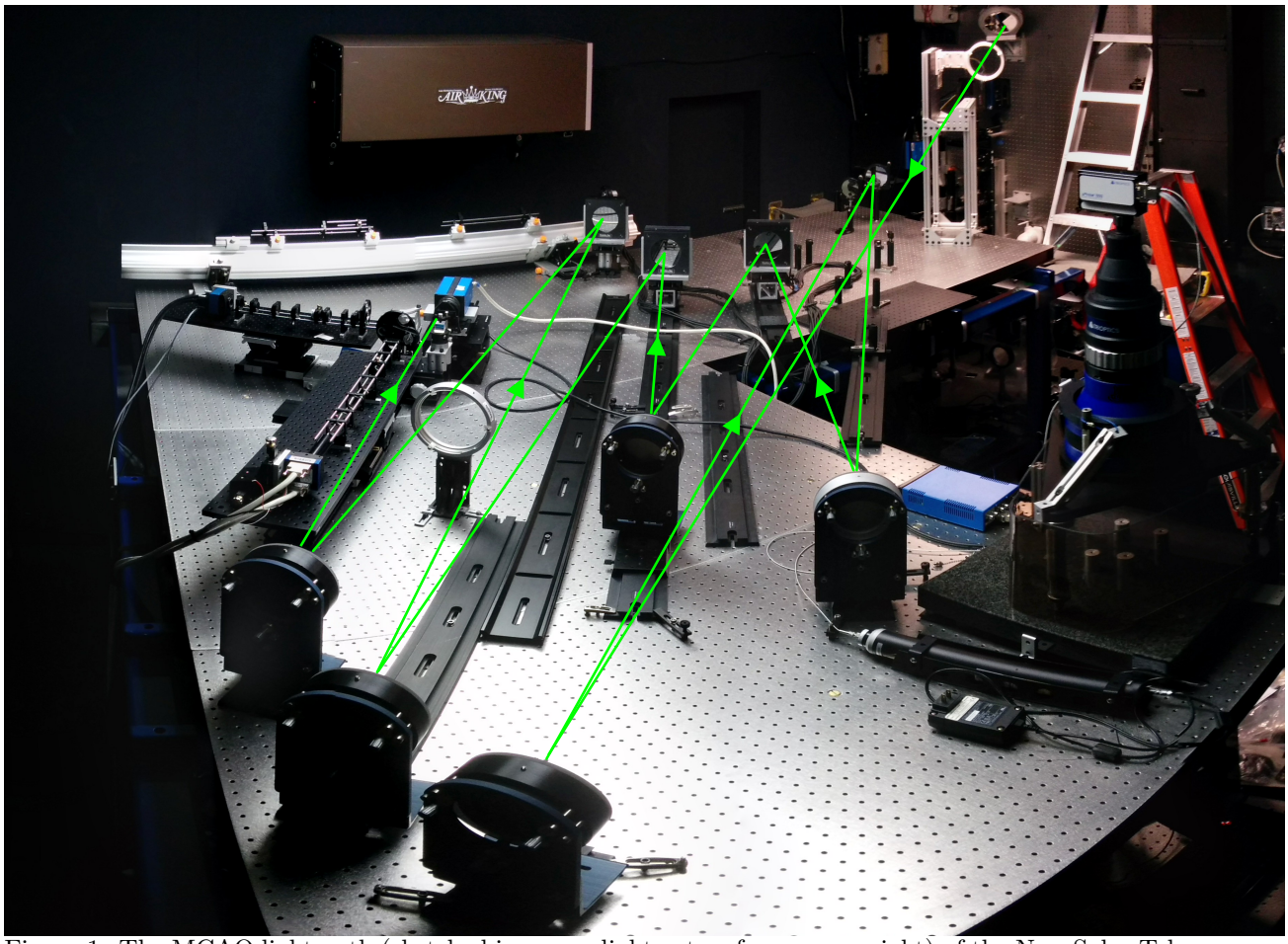

Figure 1: The MCAO light path (sketched in green, light enters from upper right) of the New Solar Telescope on May 21, 2015. This photograph shows configuration "B" (fig. 2). The black platforms on the left carry the MD-WFS and the OA-WFS-B. OA-WFS-A is mounted on the X95 rail in the background (feed optics not installed in this picture). The focal plane of the MCAO path is monitored with the large blue camera (PCO 2000) next to the MD-WFS. The black dovetail rails allow for quick adjustments of the high-altitude DMs (figs. 3 and 4).

we have to address various issues such as the relevance of the sequencing of the deformable mirrors (see references [6] p. 54, [7], [8]) for solar MCAO, and wavefront sensing schemes with our experimental system that is designed purposely to be very flexible. The initial design and some specific considerations were reported in references [5], and [9]. NST MCAO deploys three deformable mirrors (DMs), and two on-axis Shack-Hartmann wavefront sensors (OA-WFS-A and OA-WFS-B with only one being used at a time) as well as one wide-field Shack-Hartmann that is used as a multi-directional sensor (MD-WFS). The main specifications are summarized in tables 1, and 2. The control software is KAOS Evo 2, (fig. 6) which was initiated for the AO and MCAO systems of GREGOR.[10] In the initial optical design, the final focus of the NST MCAO path was merged with the telescope's original science focus. As the space at the original focus was very limited and difficult to access, in 2015, we dedicated its own focus to the MCAO. We also improved the optical quality of the path as well as the optics of the MD-WFS. The re-worked setup shows a much better image quality, and we obtained decent enough wavefront sensor signals under normal seeing conditions to close the MCAO loop.

2.1.1 Configuration options

NST MCAO allows for various basic optical configurations as enumerated in fig. 2, which will be used in experiments.

Configuration A This configuration is similar to the concept of GREGOR MCAO in which the on-axis WFS only sees $\mathrm{DM}^{\mathrm{up}}_{0\,\mathrm{km}}$, which is upstream of the high-altitude DMs. There are two motivations for the mirror sequence in this configuration: 1. early solar MCAO setups have been downstream extensions to existing CAO systems, and GREGOR MCAO followed this philosophy. 2. Correcting turbulence close to the ground with $\mathrm{DM}^{\mathrm{up}}_{0\,\mathrm{km}}$ before correcting higher turbulence is optimal as argued by [6] and [7]. The on-axis WFS does not see any high-altitude DM in order to avoid dynamic misregistration,[11] and/or dynamic vignetting of the marginal subapertures. In this configuration, OA-WFS-A forms a Fried geometry with $\mathrm{DM}^{\mathrm{up}}_{0\,\mathrm{km}}$ on the full 100-mm aperture of the DM.

Configuration B This configuration is similar to the GeMS scheme in which the pupil DM is located downstream of the high-altitude DMs without intermediate relay optics.[12] The advantage of this configuration is the simplified optics and that there is no high-altitude DM between $\mathrm{DM}_{0\,\mathrm{km}}$ and the on-axis WFS that could introduce dynamic misregistration between the two. OA-WFS-B forms a Fried geometry with $\mathrm{DM}^{\mathrm{down}}_{0\,\mathrm{km}}$, which is in the pupil image downstream of the high-altitude DMs. However, this pupil measures only 90 mm, hence only 19 of the 21 actuators across the face sheet and 18 subapertures are illuminated. That is, the subapertures are slightly bigger in this configuration, but still in a Fried geometry with $\mathrm{DM}^{\mathrm{down}}_{0\,\mathrm{km}}$. Even though, the high-altitude DMs do not disturb the Fried matching of OA-WFS-B and $\mathrm{DM}^{\mathrm{down}}_{0\,\mathrm{km}}$, they still distort the pupil image on $\mathrm{DM}^{\mathrm{down}}_{0\,\mathrm{km}}$ and in the wavefront sensor, boiling down to dynamic illumination variations for marginal subapertures. In order to escape this effect, we do not use all 18 subapertures but only 16 subapertures across the pupil and disregard one subaperture at every rim. The un-illuminated actuators of $\mathrm{DM}^{\mathrm{down}}_{0\,\mathrm{km}}$ are slaved. To clean the pupil wavefront from the uncorrected ring, we stop down a consecutive pupil image in the science path accordingly. That is, the effective telescope size in the science focus gets reduced by about 18 cm. The reason for this stop is not only to dispose of the uncorrected area, but also to circumvent intensity fluctuations ("flying shadows") in the MCAO corrected image as proposed in [13].
The switch from configuration B to A, which involves swapping the pupil DM with a flat mirror and feeding OA-WFS-A, takes us approximately one day.

Configuration B* This configuration is identical to configuration B, except that one of the high-altitude DMs is removed and placed into the first pupil image instead, such that two DMs are conjugate to the telescope pupil. The aim of this configuration is to compare the relevance of sequence of the DMs and of the dynamic misregistration to the MCAO correction by switching back and forth from one pupil DM ($\mathrm{DM}^{\mathrm{down}}_{0\,\mathrm{km}} \leftrightarrow \mathrm{DM}^{\mathrm{up}}_{0\,\mathrm{km}}$) to the other instantly, so that the other pupil DM is always passive.

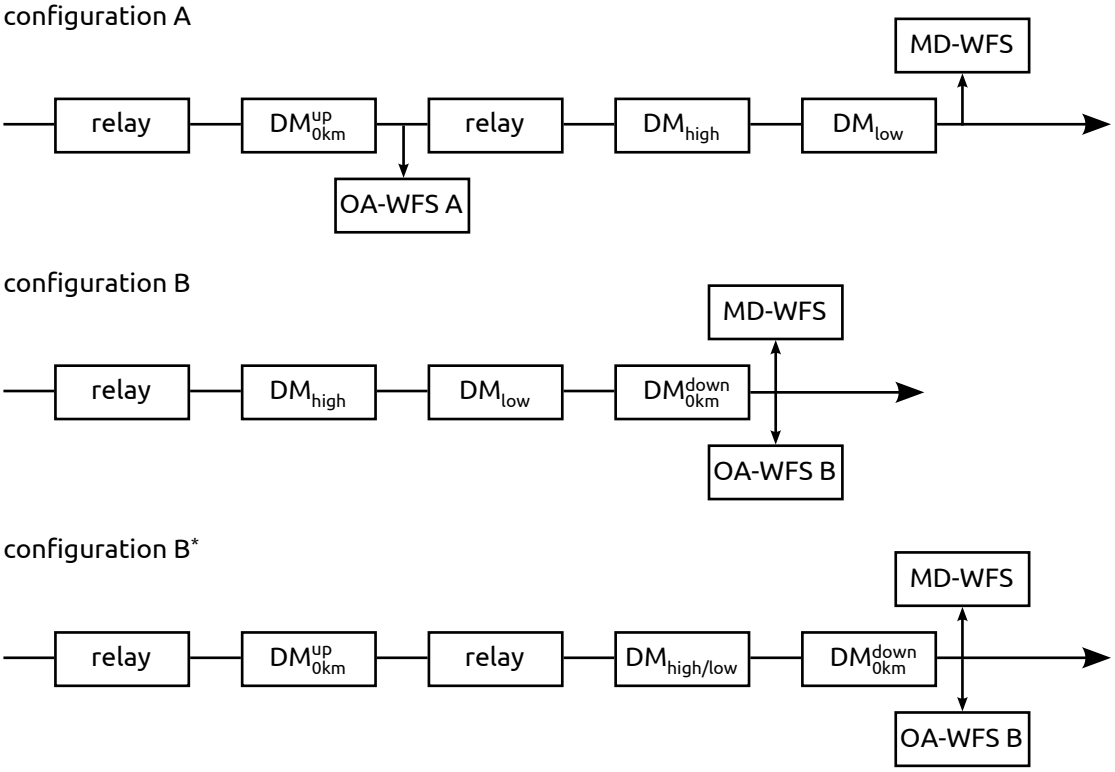

Figure 2: Optical configurations available in NST MCAO.

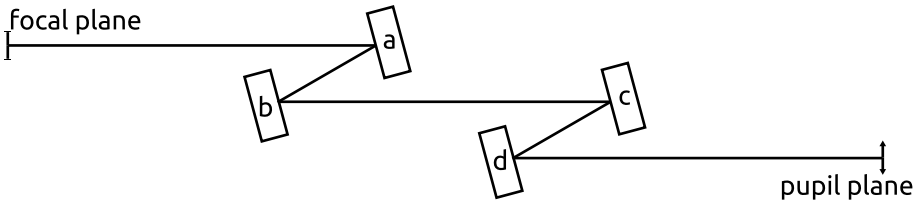

Figure 3: Schematic representation of the double-Z configuration of the high-altitude DMs. Any of the mirror positions "a", "b", "c", or "d" can be occupied either by a flat mirror or by a deformable mirror. Mirror "a" is highest (closest to infinity), and mirror "d" is lowest (closest to the pupil).

Conjugations of the high-altitude DMs The conjugate planes of the high-altitude DMs can be changed individually such that the DMs can be positioned freely between 2 and 9 km (some restrictions apply). This is realized by a double-Z design as sketched in fig. 3, and 4. The double-Z is an extension of the single-Z design of GREGOR MCAO. The four mirrors—two DMs and two flats ("a", "b", "c", and "d" in fig. 3)—are mounted on three parallel rails that feature engraved ruler marks. Moving a DM to a different conjugate is very easy. It takes us about 15 minutes including aligning and full interaction matrix acquisition. The actuator spacing projected to the conjugate planes ranges from about 14 cm to 31 cm. According to reference [14], the maximum distance of a turbulent layer from a DM with actuators spaced by d_{act} for a uniformly corrected field with diameter θ can be calculated from $\Delta h_{\max} = 1.75\, d_{\mathrm{act}}/\theta$. This criterion balances the classical fitting error (DM in a layer) and the generalized fitting error (DM off the layer). Accordingly, the effective altitude range of a DM can be regarded as $2\,\Delta h_{\max}$. With the 60 arcsec maximum guide region separation of the NST MD-WFS, this yields about $2\,\Delta h_{\max} \approx 1.7 \ldots 3.7$ km, depending on the positions of the high-altitude DMs. These numbers support the need for tunable DM positions, given that the turbulence is located in a few distinct layers within the accessible range.

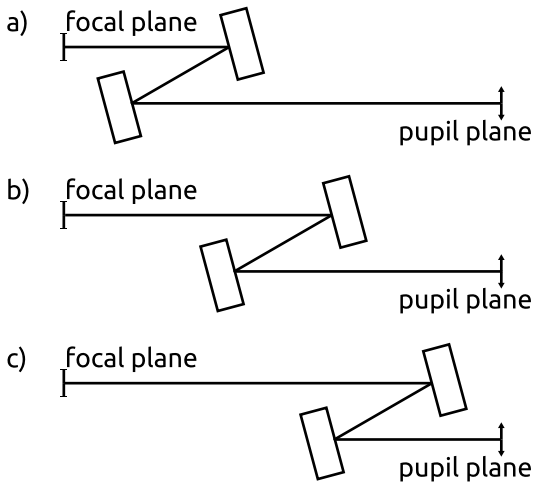

Figure 4: Altitude adjustment of the high-altitude DMs with the Z configuration. By moving both mirrors by the same distance along the parallel beams of the Z, the conjugate altitude of the mirrors can be modified without affecting the path downstream. The mirrors are moved to a higher altitude in the upper diagram (a), and to a lower altitude on the bottom (c) with respect to the central diagram (b).

	$DM_{0\,km}$	DM_{low}	DM_{high}
conjugation options	before and after DM_{low} / DM_{high}	2 to 5 km	6 to 9 km
maker	AOA Xinetics	AOA Xinetics	AOA Xinetics
type	PNM surface normal	PNM surface normal	PNM surface normal
actuators in total	357	357	357
actuators across	21	21	21
actuator spacing	5 mm	5 mm	5 mm
projected spacing	8 cm (8.9 cm in downstr. pupil)	14 cm at 2 km	31 cm at 9 km
actuators in use	357 (241 in downstream pupil)	137	137
best flat surface error	approx. 4 nm RMS	approx. 4 nm RMS	approx. 4 nm RMS

Table 1: Deformable mirrors, and conjugation options in NST MCAO. Unused actuators are slaved. All three DMs have been polished by AOA Xinetics under bias voltage.

	On-axis WFS-A	On-axis WFS-B	Multi-dir WFS
type	correlating Shack-Hartmann	correlating Shack-Hartmann	corr. Shack-Hartmann
field stop size	13″	11″	85″
guide regions	1	1	19
sub-aperture size	8.0 cm	8.9 cm	32 cm
sub-apertures across	20	16 used (18 illmuninated)	5
sub-apertures in use	308	208	19
wavelength range	(525±12.5) nm	(525±12.5) nm	(525±12.5) nm
guide region size	20×20 px	20×20 px	20×20 px
pixel scale	approx. 0.5″/px	approx. 0.5″/px	approx. 0.6″/px
DMs seen	$DM_{0\,km}$	all	all
camera	Mikrotron EoSens CL	Mikrotron EoSens CL	Mikrotron EoSens 3CL
read-out window	560×560 px	480×480 px	760×640 px
frame rate	same as MD-WFS	same as MD-WFS	1500 fps

Table 2: Wavefront sensors for NST MCAO.

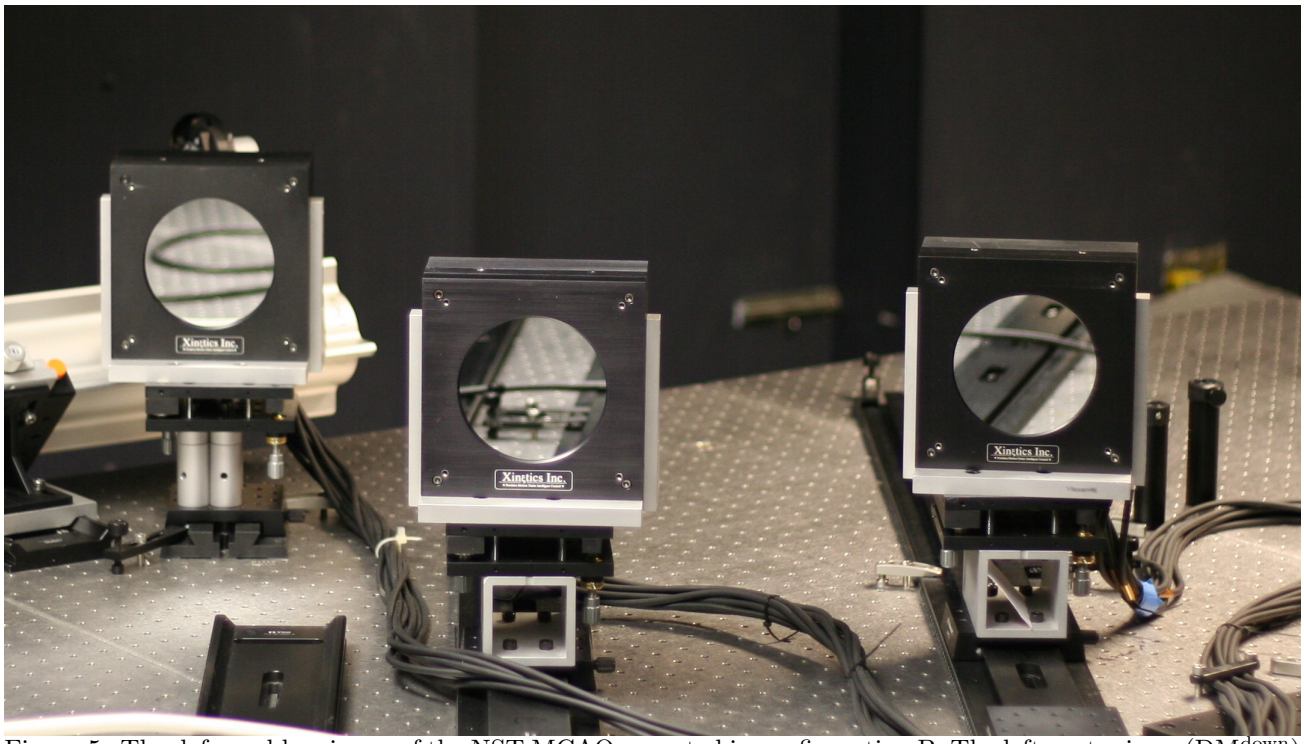

Figure 5: The deformable mirrors of the NST MCAO mounted in configuration B. The leftmost mirror ($DM^{down}_{0\,km}$) is placed in a pupil image, the central mirror (DM_{low}) is conjugate to about 3 km, and the rightmost mirror (DM_{high}) to about 7 km in this picture. The clear aperture diameter is 10 cm.

2.1.2 DM flatness

All three DMs of NST MCAO (fig. 5) are identical 357-actuator PNM mirrors made by AOA Xinetics. The DM that was delivered third (in 2013) was polished under bias voltage in the factory whereas the first two DMs were polished without voltage. These former two DMs exhibited uncorrectable high-frequency figure errors when bias voltage was applied. We had these two DMs repolished under bias voltage by AOA Xinetics in 2015. The combined Strehl ratio of all three DMs at best flat figure is now higher than 90% at 500 nm.

2.2 Experimental progress

The modifications performed in 2015 have lead to a great improvement of the optical quality of the MCAO path, and the image in the classically corrected MCAO focus is comparable to the image in the original NST AO focus. We closed the MCAO loop several times with two and three DMs. Because we haven't had any means to estimate the turbulence profile, we blindly moved the high-altitude DMs multiple times hoping to get closer to strong turbulent layers.

In figure 7, we show that the MCAO control loop could correct for an unflat DM_{high} using the Sun as reference. The amount of atmospheric correction due to MCAO has not been analyzed conclusively for this dataset as we believe that the major improvement is due to minimizing the figure error of DM_{high} in the MCAO loop. In order to compare the atmospheric correction of CAO ($DM^{down}_{0\,km}$ only) with MCAO ($DM^{down}_{0\,km}$ and DM_{low} at 2.4 km in this example), we analyzed the directional wavefront error for all guide regions based on recorded MD-WFS data. We reconstructed Karhunen-Loeve coefficients $c_{j,r}(t)$ up to mode number 35 for any control loop cycle t where j is the mode index and $r = 1 \ldots 19$ is the index of the guide region, and computed the variance

$$s_{j,r} = \frac{1}{n-1} \sum_{t=1}^{n} [c_{j,r}(t) - \bar{c}_{j,r}]^2 \tag{1}$$

Figure 8 shows the ratio

$$\frac{s_{j,r}^{\mathrm{MCAO}}}{s_{j,r}^{\mathrm{CAO}}}$$

of two approximately 30 second long time series of CAO and MCAO correction, which where taken directly after each other. The reconstructed wavefront variance is smaller with MCAO correction in every guide region, and $s_{j,r}^{\mathrm{MCAO}}/s_{j,r}^{\mathrm{CAO}}$ becomes as small as about 30% for lower modes. This improvement, however, is hard to see visually in the recorded images, and further efforts to boost the MCAO correction are planned. The undersized pupil stop in the science path after the high-altitude DMs effectively prevented apparent intensity fluctuations in the image plane caused by MCAO correction. We did not analyze the photometric stability in detail, but conclude at this point that the "flying shadows" can in fact be removed with this kind of stop.

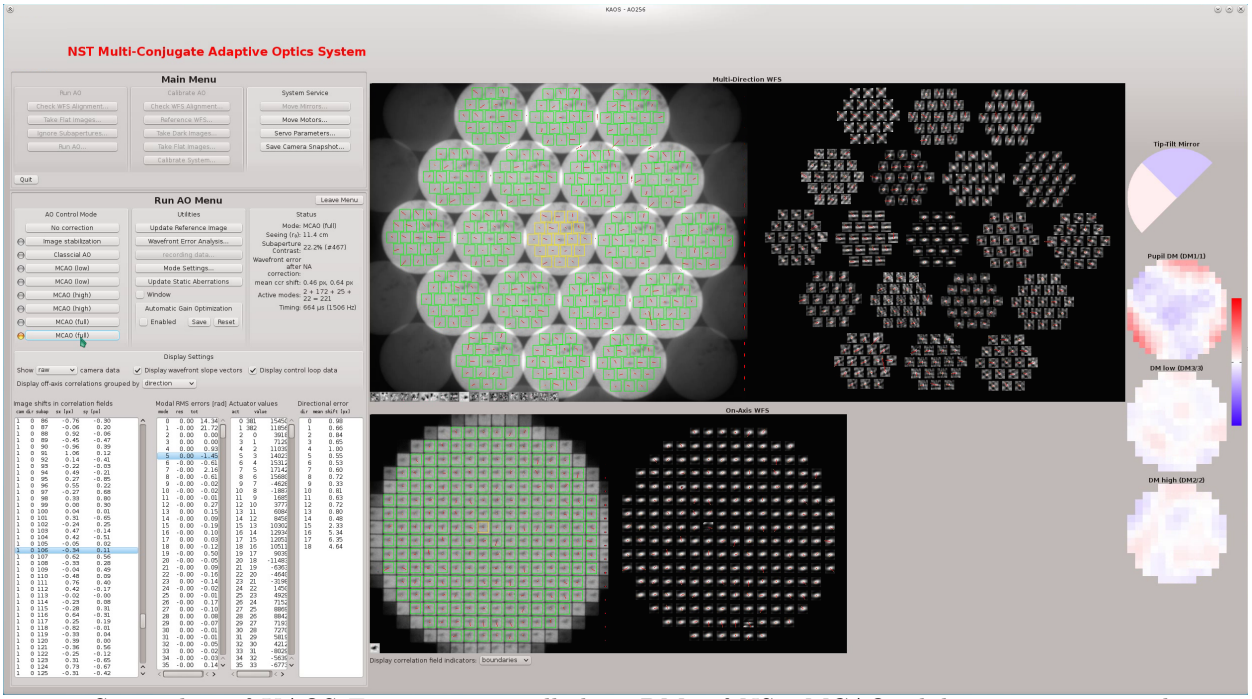

Figure 6: Screenshot of KAOS Evo 2 running all three DMs of NST MCAO while pointing at a solar active region. The WFS views show the raw camera frame and the computed cross-correlation maps. Yellow boxes indicate the guide regions.

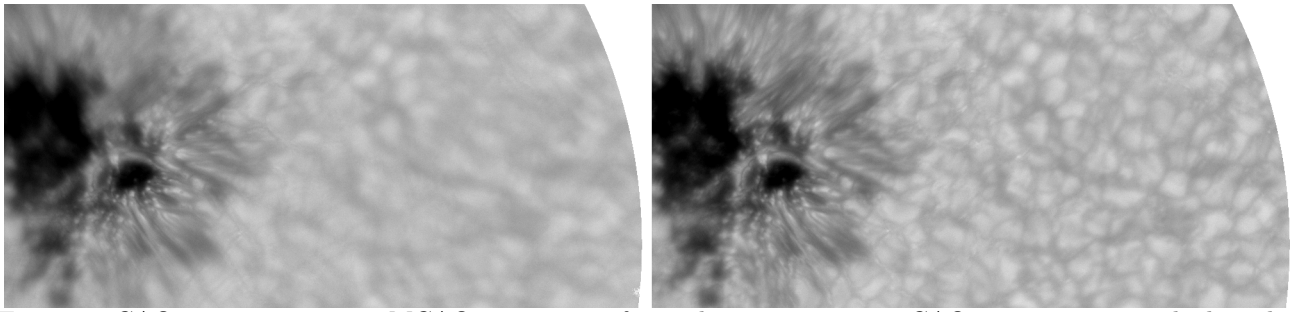

Figure 7: CAO correction versus MCAO correction of an solar active region. CAO correction is applied to the sunspot in the left picture and MCAO correction with $\mathrm{DM}_{0\,\mathrm{km}}$ and $\mathrm{DM}_{\mathrm{high}}$ at 7 km in the right picture. Both images are arbitrarily selected but represent typical snapshots of the image bursts taken. The picture on the left was degraded by $\mathrm{DM}_{\mathrm{high}}$ being purposely unflat. This error was clearly reduced by the MCAO control loop. The shown image section is about 40 arcsec wide. An interference filter at (705.7 ± 5) nm (titanium-oxide line) was used.

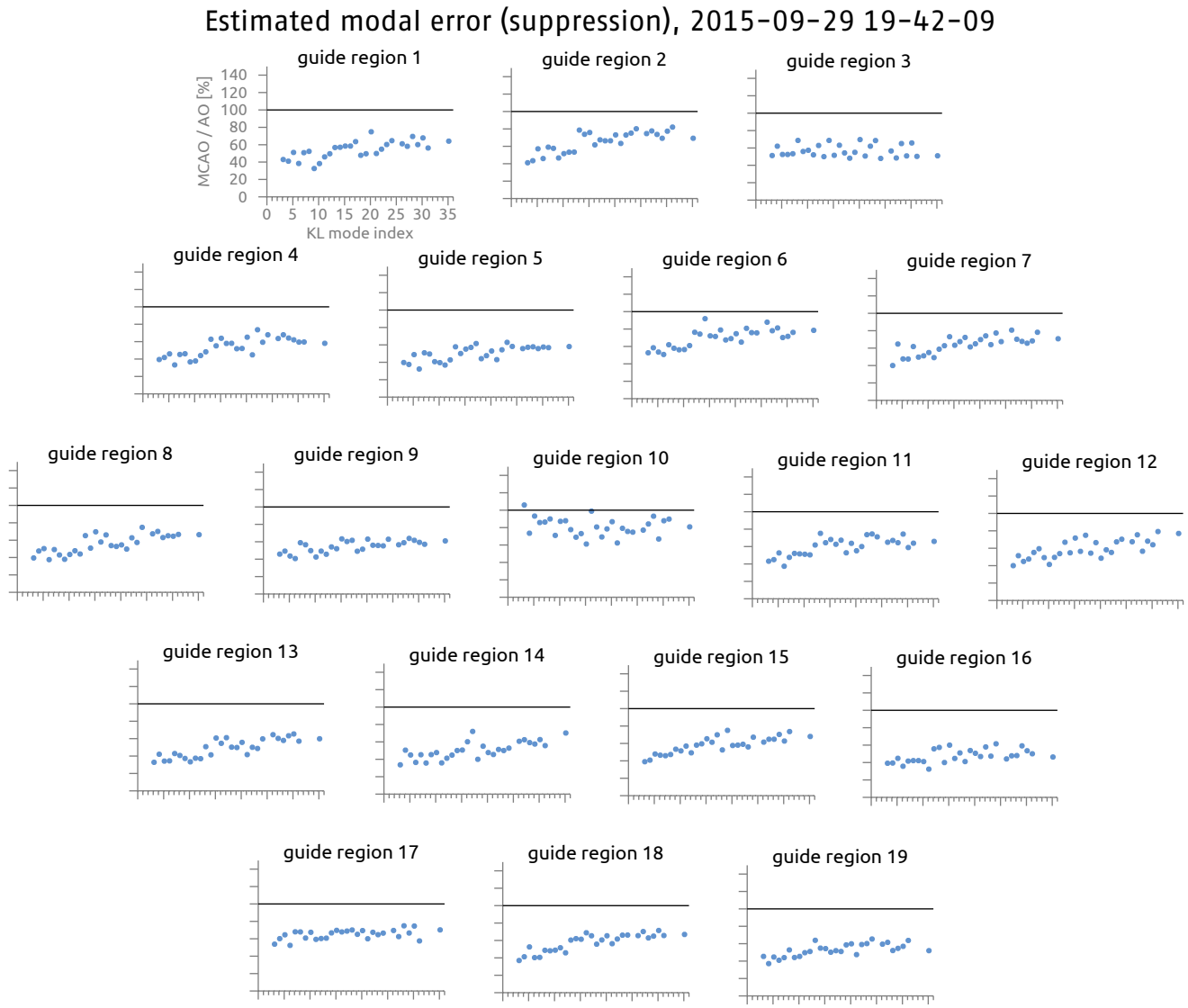

Figure 8: Correction turbulence with classical AO correction versus MCAO. This plot shows the ratio of the variances of an AO and an MCAO sequence (both 30 seconds long) of reconstructed Karhunen-Loeve coefficients for each guide region of the MD-WFS (w/o tip-tilt).

3. SUMMARY AND OUTLOOK

The MCAO system of the NST at BBSO is a very flexible pathfinder system. We showed that this system is able to compensate well for static aberrations across the field introduced by unflat DMs, while using the Sun as reference for the wavefront sensors. We also demonstrated an improvement in the variance of the wavefront modal expansion all across the field. An undersized exit pupil stop prevented intensity fluctuations in the MCAO corrected image plane. During the experiments in 2015, we had no information about the instantaneous turbulence profile. We are now collaborating with A. Guesalaga (Pontificia Universidad Católica de Chile), and B. Neichel (Aix-Marseille Université) to explore the use of their profiling tool for the present application. We are also considering new changes in the setup to improve the benefits from MCAO.

ACKNOWLEDGMENTS

We gratefully acknowledge the support of AFOSR grant FA9550-15-1-0322, NSF grants AST-ATI-1407597, AGS-1250818 and NASA grant NNX13AG14G. A number of people have contributed in various form to the NST MCAO project. We would particularly like to name and thank J. Nenow, E. Norro, R. Coulter, C. Plymate, J. Varsik, S. Shoumko (all BBSO), as well as P. Markus and A. Fischer (both KIS), and J. Doherty (NSO). We have been appreciating technical support of C. Hayes (EDT), and T. Schneider (Riptide Realtime). The lead author sincerely thanks P. Goode (BBSO), T. Rimmele (NSO), O. von der Lühe, T. Berkefeld, and D. Soltau (all KIS) for supporting the collaboration with the GREGOR MCAO project.

REFERENCES

[1] Berkefeld, T., Soltau, D., and von der Luehe, O., "Results of the multi-conjugate adaptive optics system at the German solar telescope, Tenerife," *Proc. SPIE* **5903**, 59030O–59030O–8 (2005).

[2] Rimmele, T., Richards, K., Roche, J., Hegwer, S., and Tritschler, A., "Progress with solar multi-conjugate adaptive optics at NSO," *Proc. SPIE* **6272**, 627206–627206–5 (2006).

[3] Langlois, M., Moretto, G., Richards, K., Hegwer, S., and Rimmele, T. R., "Solar multiconjugate adaptive optics at the Dunn Solar Telescope: preliminary results," *Proc. SPIE* **5490**, 59–66 (2004).

[4] Schmidt, D., Berkefeld, T., Heidecke, F., Fischer, A., von der Lühe , O., and Soltau, D., "GREGOR MCAO looking at the Sun: results with a triple conjugate adaptive optics system ," *Proc. SPIE* **9148** (2014).

[5] Schmidt, D., Gorceix, N., Zhang, X., Marino, J., Coulter, R., Shumko, S., Goode, P., Rimmele, T., and Berkefeld, T., "The multi-conjugate adaptive optics system of the New Solar Telescope at Big Bear Solar Observatory," *Proc. SPIE* **9148** (2014).

[6] Hardy, J. W., [*Adaptive Optics for Astronomical Telescopes*] (July 1998).

[7] Flicker, R. C., "Sequence of phase correction in multiconjugate adaptive optics," *Optics Letters* **26**, 1743–1745 (Nov. 2001).

[8] Montoya, L., Montilla, I., and Collados, M., "MCAO numerical simulations for EST: analysis and parameter optimisation," (2015).

[9] Zhang, X., Gorceix, N., Schmidt, D., Goode, P., Rimmele, T., Coulter, R., and Cao, W., "Optical design of the Big Bear Solar Observatory's multi-conjugate adaptive optics system," *Proc. SPIE* **9148** (2014).

[10] Berkefeld, T., Schmidt, D., Soltau, D., von der Lühe, O., and Heidecke, F., "The GREGOR adaptive optics system," *Astronomische Nachrichten* **333**, 863 (Nov. 2012).

[11] Schmidt, D., Berkefeld, T., and Heidecke, F., "The 2012 status of the MCAO testbed for the GREGOR solar telescope," *Proc. SPIE* **8447**, 84473J–84473J–11 (2012).

[12] Rigaut, F., Neichel, B., Boccas, M., d'Orgeville, C., Vidal, F., van Dam, M. A., Arriagada, G., Fesquet, V., Galvez, R. L., Gausachs, G., and 20 others, "Gemini multiconjugate adaptive optics system review - I. Design, trade-offs and integration," *Monthly Notices of the Royal Astronomical Society* **437**, 2361–2375 (Jan. 2014).

[13] von der Lühe, O., "Photometric stability of multiconjugate adaptive optics," *Proc. SPIE* **5490**, 617–624 (2004).

[14] Rigaut, F. J., Ellerbroek, B. L., and Flicker, R., "Principles, limitations, and performance of multiconjugate adaptive optics," *Proc. SPIE* **4007**, 1022–1031 (July 2000).